Praca oryginalna *Original paper*

Size of nanocrystals affects their alimentary absorption in adult mice*)

MICHAL M. GODLEWSKI*, **, JAROSLAW KASZEWSKI*, **, *****, ANNA SZAL*, **, ANNA SLONSKA*, **, MALGORZATA A. DOMINO**, ***, EWA MIJOWSKA****, BARTLOMIEJ S. WITKOWSKI*****, MAREK GODLEWSKI*****

*Department of Physiological Sciences, Faculty of Veterinary Medicine, Warsaw University of Life Sciences – SGGW, Nowoursynowska 159, 02-776 Warsaw, Poland
**Veterinary Research Centre, Faculty of Veterinary Medicine, Warsaw University of Life Sciences – SGGW, Nowoursynowska 100, 02-797 Warsaw, Poland
***Department of Large Animal Diseases with Clinic, Faculty of Veterinary Medicine, Warsaw University of Life Sciences – SGGW, Nowoursynowska 100, 02-797 Warsaw, Poland
****Institute of Chemical and Environmental Engineering, West Pomeranian University of Technology, ul. Pułaskiego 10, 70-322 Szczecin, Poland
*****Institute of Physics, Polish Academy of Sciences, al. Lotników 32/46, 02-668 Warsaw, Poland

Received 08.04.2014 *Accepted 08.07.2014*

Godlewski M. M., Kaszewski J., Szal A., Slonska A., Domino M. A., Mijowska E., Witkowski B. S., Godlewski M.

Size of nanocrystals affects their alimentary absorption in adult mice

Summary

Luminescent nanocrystals and quantum dots have great potential for use as fluorescent markers in biology and medicine. However, their first generations were based on the heavy-metal core, which was unstable and shed heavy-metal ions into biological media. This, coupled with a lack of information on their biodistribution and pharmacokinetics, rendered them unusable for purposes outside research. The recently developed non-heavy metal nanocrystals are a promising material for future medical use. Yet, the controversies over their application, absorption and biodistribution remain. Various recent papers present different results on the uptake of nanocrystals and on their intracellular and organ distribution. In our study, we focused on the question of how the size and shape of nanocrystals affect their duodenal absorption after intragastric gavage (IG) and distribution to the liver. Commercial bulk nanoparticles and hydrothermal nanoparticles produced at the Institute of Physics PAS were the same in composition and excitation-emission range, but significantly different in shape and size. Adult mice (n = 24) aged 3-6 months were kept in standard living conditions (12 h day-night cycle), fed ad libitum with unobstructed access to water. Following a 1-week adaptation period, an RO water suspension of nanoparticles (50 µg/ml) was administered by IG. No changes in the behaviour of the mice or pathophysiological changes in their organs were observed following IG. The control group received an identical volume of RO water by IG. Cross-sections of the organs were examined both qualitatively and quantitatively by confocal microscopy and scanning cytometry. Following IG, both types of nanoparticles entered the duodenum in a similar time, but only the smaller, elongated hydrothermal nanoparticles were absorbed through the intestinal epithelium and distributed throughout internal organs ($p \leq 0.001$). In conclusion, we found that the size and shape of nanocrystals is crucial for their bioavailability.

Keywords: rare-earth nanocrystals, gastrointestinal uptake, persorption

Luminescent nanocrystals and quantum dots show great potential for use as fluorescent markers in biology and medicine. Preliminary results have been encouraging and show the visualising properties of quantum dots in the diagnosis of tumours (1, 6, 10, 31). However, the first generations of nanocrystals were based on a heavy-metal core, which was unstable and shed heavy-metal ions into biological media (8). This, coupled with a lack of information on their biodistribution and pharmacokinetics, rendered them unusable for purposes outside research. Thus the search started for a non-heavy metal solution for highly fluorescent nanocrystals. Recently developed rare-earth-doped nanocrystals are a promising material

*) This study was partially financed with the grant Innovative Economy (POIG.01.01.02-00-008/08) from the European Regional Development Fund of the European Union and with the grant DEC-2012/05/E/NZ4/02994 from the National Science Centre.

for future medical use (14, 22, 27). They were screened for a high fluorescent yield and the excitation-emission constraints of typical research and medical microscopy systems (22, 27, 33). Following the initial success of the uptake of nanoparticles (5, 15), further development emphasised the shift of the excitation range to a highly penetrative infrared and the optimisation of fluorescence intensity. Nevertheless, the controversies over the route of application of nanocrystals, as well as the mechanism of their absorption and biodistribution remain. The gastrointestinal uptake of fluorescent, rare-earth-doped nanoparticles has already been described (14). Following intra-gastric gavage (IG), nanocrystals were quickly absorbed through the small intestine epithelium and rapidly (within 24 h) distributed to the majority of organs and tissues, including the brain. It is postulated that the intestinal absorption of nanocrystals in the adult gut is based on the same mechanisms as the persorption of other large and bioactive molecules (11). Up to date, three routes of persorption have been described. First, through the uptake of antigens and antigen-antibody complexes, involves intestinal M cells and is highly unlikely for nanocrystals (34). Second, through lesions in the continuity of the epithelial layer and through the extrusion zone (17, 29), does not explain the observed distribution pattern of nanocrystals in enterocytes and would be insufficient for the observed scale of uptake (14). Final, and the most probable, is the transcellular route (for details see 14). Still, little is known about the actual process through which fluorescent nanocrystals enter the enterocyte. Three processes of the uptake of bulk material from outside of the cell are known and postulated for the uptake of nanocrystals. Endocytosis is a highly specific process requiring receptor-ligand interaction and the involvement of clathrins in the invagination of the cell membrane and the internalisation of a thus-created vesicle in the cell (20). A rough estimate of the diameter of a particle capable of entering the cell in this way is 100 nm. The second uptake mechanism is the non-specific pinocytosis (15). This caveolin-mediated system of intracellular transport is characteristic of the uptake of water and ions, and the largest possible diameter of particles in this process is 50 nm (20). The third possibility is the so-called macropinocytosis, characteristic of the internalisation of macroviruses (9, 25, 28, 32). Although it requires the formation of lipid rafts and receptor-ligand interaction, this process is much less specific than endocytosis and may explain the passage of particles as large as 500-5000 nm (20). Considering the alternatives, this could be the way for crystalline structures to enter enterocytes. The remaining issue is the actual size of the alleged nanomaterials and quantum dots. In biology and medicine, the size is of great importance because it determines not only the possibility of the uptake of a given nanomaterial, but also its pharmacokinetics and intracellular distribution pattern (14). From the physical point of view, 10 nm is an absolute limit for the quantum effect observed in nanomaterials (30). The interaction intensity related to the effect may be weak, intermediate or strong, depending on the relationship between the radius of the particle and the Bohr radius of the bulk exciton (23). Aggregates or polycrystalline substances consisting of many "nano-domains" may retain the quantum effects. Additionally, the agglomeration of semiconductor quantum dots was reported to enhance the luminescence properties of the material (21).

The aim of this study was to evaluate the effect of the size and shape on nanoparticles on their gastrointestinal uptake and biodistribution in the organism.

Material and methods

Alcohols, paraformaldehyde and xylene were purchased from Avantor Performance Materials Poland S.A. (Gliwice, Poland). Unless stated otherwise, all other media and reagents were purchased from Sigma-Aldrich Sp. z o.o. (Poznań, Poland).

Preparation of nanocrystals. Polycrystalline Y_2O_3:Eu powder was purchased from a commercial supplier. Hydrothermal Y_2O_3:Eu nanoparticles, with the same chemical composition as the commercial ones, were produced at the Institute of Physics PAS by methodology similar to that described in (33). The concentration of Eu in the samples was set at 4% mol. The hydrothermal nanopowder was prepared by precipitation from a watery nitrate (V) solution of Y and Eu ions. The obtained residue was processed in a microwave hydrothermal reactor at a pressure of 6 MPa. The microwave hydrothermal process was used to obtain a narrow distribution of the grain sizes of the nanoparticles produces. Pure cubic Y_2O_3:Eu nanopowder was synthesized in the form of needle-like particles. The wet product was then dried and calcined at 1000°C in a ceramic boat to promote recrystallisation and to optimise its structural biocompatibility (Fig. 1).

Physical characterization of Y_2O_3:Eu nanocrystals. Detailed structural and morphological analyses, as well as photoluminescence measurements, of the nanocrystalline Y_2O_3:Eu samples were performed. Transmission electron microscopy (TEM) measurements were performed with a Tecnai F30 transmission electron microscope (FEI, Brno,

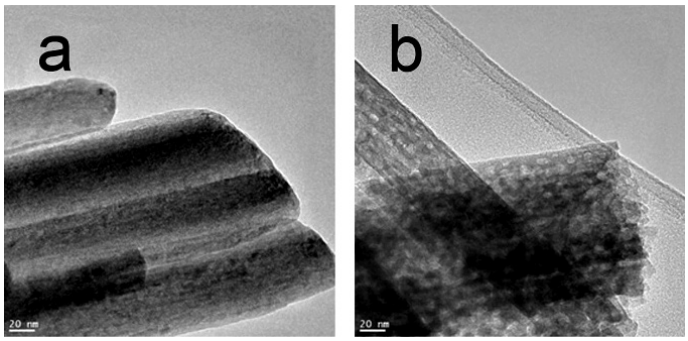

Fig. 1. Calcination of Y_2O_3:Eu nanocrystals created by the hydrothermal method, visualised by TEM; a) monocrystaline nanoparticles prior to thermal annealing; b) nanoparticles after the process of thermal annealing at 1000°C, note the abundance of nanodomains (examples indicated by arrows) formed during the recrystallization process

Czech Republic), operating at 200 kV. Powder samples were prepared by dispersion of dry powders in acetone using an ultrasound bath for 30 min. Then the suspension was dropped on a copper grid (200 mesh) with polycarbonate coating and hotplated for 2 h. Photoluminescence excitation spectra (PLE) were measured at room temperature with a Solar CM 2203 spectrofluorimeter (SOLAR, Belarus) with emission set at 613 nm while excitation ranged from 220 to 500 nm. Scanning electron microscopy (SEM) measurements were performed with a Scanning Electron Microscope SU-7 (Hitachi, San Jose, CA, USA). Powder samples were suspended in distilled water with a VCX-500 ultrasound system (Sonics&Materials, Inc., Newtown, CT, USA), dropped on a silicon monocrystalline wafer, and then dried at 40°C before observation.

Animals. All experiments were approved by the local ethical committee (LEC agreement No 44/2012). Adult male Balb-c mice (n = 24) aged 3-6 months were kept in standard living conditions (12 h day-night cycle), fed *ad libitum* with unobstructed access to water. Following a 1-week adaptation period, a freshly prepared RO water suspension of nanoparticles (50 µg/ml) was administered via intragastric gavage (IG, 0.3 ml/mouse). No behavioural changes or discomfort were observed in the animals after the procedure. Following IG, the mice were kept for the experiment-imposed period and then sacrificed by an overdose of barbiturates. All internal organs, blood, bile, as well as muscle and fat tissues, were collected for future analyses.

Tissue processing and analyses. Organs and tissues for the experiments were fixed for 24 h in 4% buffered paraformaldehyde, and then transferred to 70% ethanol for storage until the embedment procedure. Fixed tissues were dehydrated in a series of alcohol concentrations and embedded in paraffin with a STP 120 tissue processor (Microm, Walldorf, Germany) according to the standard histological procedure. Embedded tissues were then cut into 5 µm-thin sections with an HM 325 rotary microtome (Microm, Walldorf, Germany) and fixed to silane-coated microscope slides (Equimed Sp. J. Warsaw, Poland). Samples were then deparaffined in xylene and rehydrated in a series of alcohol solutions according to the standard histological procedure. Then the slides were rinsed in PBS and boiled three times in a 500 W microwave in a phosphate buffer for antigen retrieval. After cooling down, the samples were rinsed in PBS for 5 min. For a simple evaluation of the Y_2O_3:Eu distribution and for scanning cytometry, cell nuclei were counterstained with HOECHST 33342 (0.1 mg/ml, 2 min.). For immunofluorescence, samples were incubated for 30 min. with 5% goat serum (GS) to block unspecific binding epitopes. Then, cross-sections were labelled with either primary rabbit anti-CPP32 antibodies (Santa Cruz Biotechnology Inc., Dallas, TX, USA) 1: 100 in PBS-5%GS or primary mouse anti-CD45 antibodies (AbD Serotec, Oxford, UK) 1: 200 in PBS-5%GS followed by secondary chicken anti-rabbit Alexa Fluor 488-conjugated antibodies (AF488; Life Technologies Polska Sp. z o.o., Warsaw, Poland) 1: 250 in PBS. All incubations were carried out for 1 h at room temperature in a dark, humidified incubation chamber. Between the steps, samples were rinsed twice in PBS. Finally, after another rinse in PBS, a mounting medium for immunofluorescence was added prior to the application of coverslips (Gerhard Menzel GmbH, Braunschweig, Germany). For Y_2O_3:Eu, 488 nm excitation vs. a 560IF emission filter was used. For HOECHST 33342, 405 nm excitation was used against a 430IF emission filter. For AF488, 488 nm excitation *vs.* a 505-525 filter was used. Because of the possible overlap of fluorescence channels, the sequence scan mode was employed. Specimens were visualised under a FV-500 confocal microscope (Olympus-Polska Sp. z o.o., Warsaw, Poland). Quantitative evaluation was performed under a SCAN^R scanning cytometer (Olympus Polska). Cells were identified on the basis of the outline of nuclei labelled with HOECHST 33342. Cell-related CD45 and Y_2O_3:Eu fluorescence was evaluated from the region within 10 pixels from the nucleus contour. The index of cells positive for CD45 and Y_2O_3:Eu was calculated from the total number of cells identified separately for each cross-section. One slide from each organ was evaluated for pathological changes. No signs of inflammation or an abnormal accumulation of white blood cells was observed.

Statistical evaluation was performed by Graph-Pad In-Stat software (San Diego, CA, USA). The One-way Analysis of Variance (ANOVA) was performed, followed by the Tukey-Kramer Multiple Comparisons Test, with $p \leq 0.05$ considered significant and $p \leq 0.001$ as highly significant.

Results and discussion

Optical and physical characterisation of commercial and hydrothermal Y_2O_3:Eu nanoparticles. Characterisation of the nanoparticles was performed at the Institute of Physics, PAS. The excitation spectra analyses (PLE) revealed similarities between the commercial and hydrothermal Y_2O_3:Eu resulting from the intra-4f6 luminescence transitions within Eu^{3+} ions. The intensity relationship between emission lines was preserved in both samples, but the commercial sample exhibited a higher overall integral fluorescence yield in the whole examined range (Fig. 2a). The SEM images of Y_2O_3:Eu show the differences in the shape and size of the particles. The commercial powder contained spherical grains with rough sizes from about 10 to several dozen µm. In contrast, the microwave hydrothermal nanopowder consisted of needle-like grains with a width of 100-500 nm and length between 1 and a few µm (Fig. 2, compare b and c). Although the hydrothermal nanoparticles exhibited a much greater size standardisation, they were not uniform in their internal structure, as was found after TEM observations (Fig. 1b). Inserts (Fig. 2b and c) show nanoparticles evaluated under a confocal microscope with 488 nm excitation. The overall relative intensity was higher for the commercial Y_2O_3:Eu, equalled only by the aggregates of hydrothermal nanocrystals. Most of the hydrothermal Y_2O_3:Eu particles showed only a fractional fluorescent yield, in correspondence with the PLE analyses (Fig. 2a).

Qualitative evaluation of the absorption of Y_2O_3:Eu nanoparticles. Following IG, both commercial and hydrothermal nanoparticles entered the

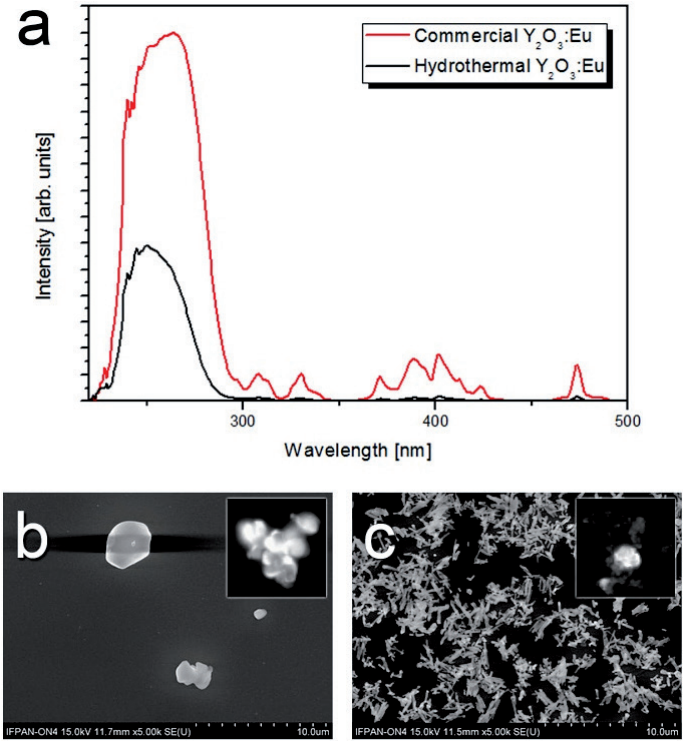

Fig. 2. Physical characterisation of commercial and hydrothermal Y_2O_3:Eu nanocrystals; a) difference in the intensity of the PLE profile between commercial (red line) and hydrothermal (black line) nanoparticles; differences in the size and shape between commercial (b) and hydrothermal (c) Y_2O_3:Eu nanocrystals visualised with a scanning electron microscope; inserts show the nanoparticles embedded in the mounting medium and visualised by confocal microscopy (60 × oil immersion lens)

duodenum in a similar time, within 1 hour (data not shown). However, 24 h after IG, the absorption and internal distribution of nanocrystals was observed only for the hydrothermal Y_2O_3:Eu (Fig. 3). Red fluorescence from the commercial nanoparticles was present only on the surface of enterocytes within the brush-border (Fig. 3a). Hydrothermal Y_2O_3:Eu was absorbed through the intestinal epithelium with a distinct granular pattern of red nanoparticle-associated fluorescence present throughout enterocytes, excluding nuclei (Fig. 3d). Similar results were obtained from the liver, with a granular pattern of the hydrothermal Y_2O_3:Eu-related fluorescence in the majority of hepatocytes (Fig. 3e). On the other hand, only a few of the red-fluorescent aggregates were observed in the case of the commercial nanoparticles (Fig. 3b). Cross-sections of the duodenum from animals that had received either the commercial or hydrothermal nanoparticles were also evaluated for the presence of apoptotic cells (Fig. 3c and f). No difference in the apoptotic index was observed between the groups, and the overall intensity of the process did not exceed the typical extent of apoptosis in the adult intestine (asterisk).

Quantitative evaluation of the absorption of the commercial and hydrothermal Y_2O_3:Eu nanoparticles. To verify the observations from confocal microscopy, cross-sections of the duodenum and liver from mice receiving both forms of nanoparticles were quantitatively evaluated by scanning cytometry. The results show a significantly higher index of cells that internalised hydrothermal nanoparticles compared with their commercial counterparts (see Tab. 1 and 2). The index of CD45-positive cells (leukocytes) was concurrently evaluated to check for inflammatory processes. Although, the incidence of CD45-positive cells in the duodenum (Tab. 1) and liver (Tab. 2) was slightly higher for the commercial nanoparticles, it did not differ significantly from that for the hydrothermal ones. Following reports of the role of granulocytes and macrophages in the uptake and circulation of quantum dots and other crystalline substances, we assessed the index of liver leukocytes involved in the uptake of circulating Y_2O_3:Eu nanoparticles. For both types of nanocrystals, the evaluated indexes did not exceed 1.5% of CD45-positive cells (Tab. 2).

Our study was prompted by discrepancies in the literature with regard to the penetration properties of various nanoparticles and their distribution pattern in

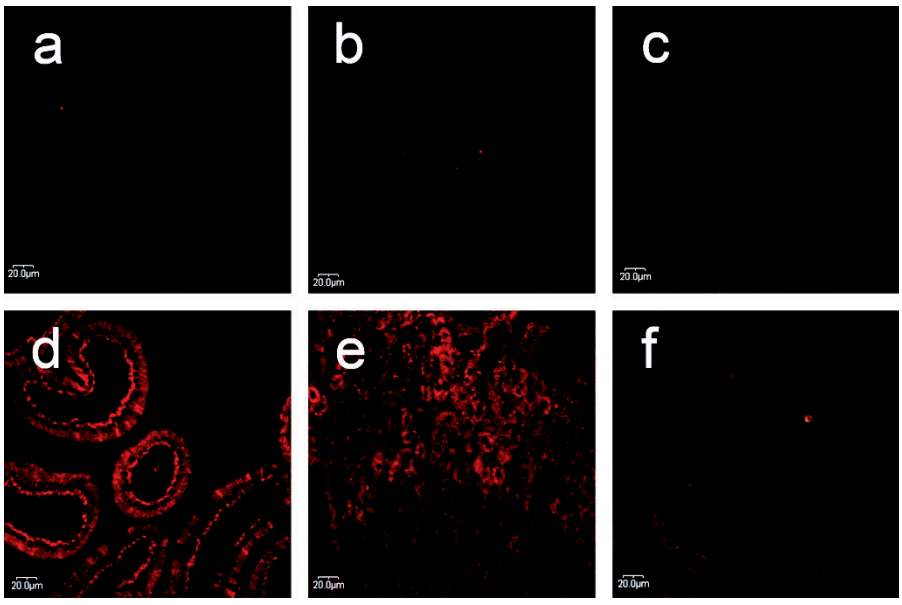

Fig. 3. Duodenal absorption (a and d) and the distribution to the liver (b and e) of the commercial (a-c) and hydrothermal (d-f) Y_2O_3:Eu nanocrystals visualised by confocal microscopy (40 × lens) 24 h after IG. Y_2O_3:Eu nanocrystals are clearly visible within the enterocytes of the duodenum and hepatocytes only in the case of hydrothermal nanoparticles – red fluorescence (compare d and e with a and b). The trace of fluorescence emitted by the commercial Y_2O_3:Eu nanocrystals can just be observed on the outside of the duodenal mucosa in the brush-border layer (a), with just single aggregates of the commercial nanocrystals present in the liver (b). Evaluation of the intensity of the apoptosis process in the duodenum exposed to Y_2O_3:Eu nanocrystals (c and f). In both cases only single apoptotic enterocytes were observed (visualisation of active caspase 3 by green fluorescence of AF488 – asterisk)

Tab. 1. Differences in the duodenal uptake of the commercial and hydrothermal Y_2O_3:Eu nanocrystals

Duodenum	Commercial	Hydrothermal	Significance
nanocrystals uptake (%)	5.14 ± 2.00	49.40 ± 5.36	p < 0.001
CD45-positive index (%)	4.04 ± 0.64	3.13 ± 1.01	n/s

Tab. 2. Differences in the index of liver cells participating in the uptake of the commercial and hydrothermal Y_2O_3:Eu nanocrystals

Liver	Commercial	Hydrothermal	Significance
nanocrystals uptake (%)	3.11 ± 2.70	14.79 ± 7.72	p < 0.001
CD45-positive index (%)	4.14 ± 1.43	2.88 ± 0.56	n/s
nanocrystals uptake by CD45-positive cells (%)	1.10 ± 0.21	1.30 ± 0.12	n/s

the organism (1, 5, 7, 10, 16, 19, 24, 26). We focused on establishing whether the size and shape of nanocrystals affects their bioavailability and distribution kinetics after alimentary application. The biocompatibility and intestinal absorption of the new generation of rare-earth-based fluorescent nanocrystals has already been confirmed. We found that, following IG, hydrothermally created ZrO_2:Pr nanoparticles were quickly absorbed by the duodenal epithelium and rapidly (within 24 h) distributed to the liver and later throughout the organism (14). In the present study we used Y_2O_3:Eu nanocrystals created by the same method. Eu doping has a major advantage over Pr doping: its emission range in red. After 488 nm excitation, ZrO_2:Pr exhibits predominantly green fluorescence, similar to the autofluorescence of tissues. Results presented in this paper describe differences in the intestinal uptake and liver content between two batches of Y_2O_3:Eu nanoparticles that were identical in their chemical composition and luminescence profile, but different in shape and size. Furthermore, the commercial sample exhibited a higher overall integral emission intensity. It seems that larger yttria crystals enabled more activator substitution sites, resulting in a higher quantity of luminescence centres. PLE spectra (Fig. 2) revealed that a charge transfer band (CTB) is active in both Eu-doped yttrium oxides. CTB results from the electronic transition from the 2p orbital of the oxygen ion to the 4f orbital of the trivalent europium ions (18). Additionally, both samples could be excited because of $4f^6$ Eu^{3+} intrashell transitions. CTB is active below 300 nm as the broad feature, numerous 4f-4f transitions are present in the range of 300-500 nm, with the highest peaking at 473 nm (blue range). The excitation of the 613 nm emission line was more effective in the commercial Y_2O_3:Eu sample in the case of CTB, as well as intrashell transitions. To improve the fluorescent yield from the hydrothermal nanoparticles, heating cycles were applied to rearrange their crystallinity. Calcination at 1000°C resulted in full recrystallisation with nanometer-size grains filling all the volume of the needle-like Y_2O_3:Eu particles (Fig. 1). This recrystallisation process virtually transformed the single crystalline structure of yttrium oxide into the tightly joined mass of true quantum dots with their greatly increased fluorescence governed predominantly by quantum effects. Although, the resulting nanoparticles reformed during the thermal annealing process, they were still structurally solid and resisted all attempts at disassociating them (data not shown). During the course of the biological experiment, we observed that even though the larger, commercial nanocrystals presented a significantly higher fluorescent yield (Fig. 2a), their uptake by duodenal enterocytes was negligible, even 24 h after IG (Fig. 3d and Tab. 1). Furthermore, for the hydrothermal Y_2O_3:Eu, a clear intracellular pattern of an uneven distribution of nanocrystal aggregates was observed. This strongly suggests the involvement of active transport for their intracellular trafficking, similar to that observed in earlier experiments, both in the mouse duodenum and in filamentous fungi (14). Even though quantum dots and nanoparticles have been postulated for applications in biology and medicine since the 1980s, few authors have studied their behaviour in a living organism. Most of their studies were conducted with the intravenous (IV) application of nanocrystaline substances (1, 6, 10, 16, 19, 26). In a few instances in which the alimentary uptake was reported, the authors only noted the appearance of the applied substances in blood (5, 24). Examples of a few thoroughly considered experiments were presented by Baek et al (3) and by Hillyer and Albrecht (15). Baek et al showed a pattern of zinc distribution throughout the organism after the alimentary application of ZnO nanoparticles. Although their results were interesting, the problem with their approach was the instability of ZnO in biological media (4, 13). Second paper evaluated the uptake and distribution of nano-gold particles of different sizes ingested by mice in drinking water. The authors showed the presence of nano-gold in the lungs, heart, kidneys, spleen, liver, gastrointestinal tract and, to a lesser extent, in the brain, with a clear preference for smaller particles. This would seem in accordance with our observations, yet gold particles used in their study were 4-58 nm, that is, much smaller than the hydrothermal Y_2O_3:Eu nanocrystals. Furthermore, TEM images presented by Hillyer and Albrecht showed a totally random distribution of gold particles throughout cell compartments, including nuclei. This observation was supported by research on cell lines (2). Together with our results and an earlier study on filamentous fungi (14) this phenomenon suggests an even greater significance of the size of nanoparticles for their uptake chance and further intracellular and intra-organism trafficking. It seems, that the smallest nanoparticles enter the cell by either simple diffusion or pinocytosis and, undetected

by cell transport systems, disseminate throughout random cellular compartments. Larger particles enter the cell by either endocytosis or macropinocytosis and are trafficked within the cell by intracellular machinery to their destination (or exit) points (14). This explains nanoparticle uptake (Tab. 1, Fig. 3d) and trafficking between different regions and organs in the body, and facilitates the observed distinct distribution (Tab. 2, Fig. 3e) and redistribution phases (14). Still larger nanoparticles cannot enter enterocytes as the size limit for bulk intracellular transport is considered to be roughly 500 nm (12). This may also answer the question raised by early research, where relatively large complexes of a nanoparticle core-shell structure with associated biomolecules were introduced into the organism IV (1, 10, 16). Authors observed a strict association of nanoparticle accumulation and transport with mononuclear phagocytes. There, the probable mechanism of the uptake of nanoparticles was based on phagocytosis, in which size limits often exceed 500 nm (12). Contrary to those observations, we did not find an accumulation of CD45-positive cells in tissues involved in the uptake (Tab. 1) and distribution (Tab. 2) of the hydrothermal Y_2O_3:Eu nanoparticles. Moreover, we did not observe a preference in the uptake of nanoparticles by the CD45-positive cells; on the contrary, only around 1% of them proved Y_2O_3:Eu-positive (Tab. 2).

The present study yielded the following conclusions:

1. Hydrothermal Y_2O_3:Eu nanocrystals were easily absorbed via the intact gut barrier in adult mice. This suggests a relatively easy method of their application as biomarkers for research and medical purposes.

2. The intestinal absorption of Y_2O_3:Eu nanocrystals depended on their size and shape, with the prerequisite of at least one dimension being in the nanoscale.

References

1. *Akerman M. E., Chan W. C., Laakkonen P., Bhatia S. N., Ruoslahti E.*: Nanocrystal targeting in vivo. Proc. Natl. Acad. Sci. USA. 2002, 99, 12617--12621.
2. *Babic M., Horak D., Trchova M., Jendelova P., Glogarova K., Lesny P., Herynek V., Hajek M., Sykova E.*: Poly(L-lysine)-modified iron oxide nanoparticles for stem cell labeling. Bioconjug. Chem. 2008, 19, 740-750.
3. *Baek M., Choi S. J., Choy J. H., Chung H. E., Jeong J., Kim T. H., Lee J. K., Lee J., Lee W. J., Oh J. M., Paek S. M., Yu J.*: Pharmacokinetics, tissue distribution, and excretion of zinc oxide nanoparticles. Int. J. Nanomed. 2012, 7, 3081-3097.
4. *Bian S. W., Mudunkotuwa I. A., Rupasinghe T., Grassian V. H.*: Aggregation and dissolution of 4 nm ZnO nanoparticles in aqueous environments: influence of pH, ionic strength, size, and adsorption of humic acid. Langmuir. 2011, 27, 6059-6068.
5. *Bockman J., Lahl H., Eckert T., Unterhalt B.*: Blood titanium levels before and after oral administration titanium dioxide. Pharmazie. 2000, 55, 140-143.
6. *Chen H., Li L., Cui S., Mahounga D., Zhang J., Gu Y.*: Folate conjugated CdHgTe quantum dots with high targeting affinity and sensitivity for in vivo early tumor diagnosis. J. Fluoresc. 2011, 21, doi: 10.1007/s10895-010-0772-4
7. *Chen N., He Y., Su Y., Li X., Huang Q., Wang H., Zhang X., Tai R., Fan C.*: The cytotoxicity of cadmium-based quantum dots. Biomaterials. 2012, 33, 1238--1244.
8. *Cho S. J., Maysinger D., Jain M., Roder B., Hackbarth S., Winnik F. M.*: Long-term exposure to CdTe quantum dots causes functional impairment in live cells. Langmuir 2007, 23, 4, 1974-1980.
9. *Daniels S. I., Soule E. E., Davidoff K. S., Bernbaum J. G., Hu D., Maeda K., Stahl S. J., Naiman N. E., Waheed A. A., Freed E. O., Wingfield P., Yarchoan R., Davis D. A.*: Activation of virus uptake through induction of macropinocytosis with a novel polymerizing peptide. FASEB J. 2014, 28, doi: 10.1096/fj.13-238113
10. *Gao X.*: Multifunctional quantum dots for cellular and molecular imaging. Conf. Proc. IEEE Eng. Med. Biol. Soc. 2007, p. 524-525.
11. *Gardner M. L. G., Steffens K. J.* (eds.): Absorption of orally administered enzymes. Springer-Verlag Berlin Heidelberg 1995.
12. *Ghigo E.*: A dilemma for viruses and giant viruses: which endocytic pathway to use to enter cells? Intervirology 2010, 53, doi: 10.1159/000312912
13. *Gilbert B., Fakra S. C., Xia T., Pokhrel S., Mädler L., Nel A. E.*: The fate of ZnO nanoparticles administered to human bronchial epithelial cells. ACS Nano. 2012, 6, 4921-4930.
14. *Godlewski M. M., Godlewski M.*: Superradiant rare-earth doped nanocrystals in the study of persorption processes in the adult intestine, [in:] Méndez-Vilas A. (ed.): Current Microscopy Contributions to Advances in Science and Technology, Microscopy Book Series #5, Formatex, Spain 2012, 582-590.
15. *Hillyer J. F., Albrecht R. M. J.*: Gastrointestinal persorption and tissue distribution of differently sized colloidal gold nanoparticles. Pharm. Sci. 2001, 90, 1927-1936.
16. *Jackson H., Muhammad O., Daneshvar H., Nelms J., Popescu A., Vogelbaum M. A., Bruchez M., Toms S. A.*: Quantum dots are phagocytized by macrophages and colocalize with experimental gliomas. Neurosurgery 2007, 60, 524-530.
17. *Kitagawa H., Yoshizawa Y., Yokohama T., Takeuchi T., Talukder M. J., Shimizu H., Ando K., Harada E. J.*: Persorption of bovine lactoferrin from the intestinal lumen into the systemic circulation via the portal vein and the mesenteric lymphatics in growing pigs. Vet. Med. Sci. 2003, 65, 567-572.
18. *Li J.-G., Ishigaki T.*: One-step Ar/O2 thermal plasma processing of Y2O3:Eu3+ red phosphors: Phase structure, photoluminescent properties, and the effects of Sc3+ codoping. Solid State Chem. 2012, 196, 58-62.
19. *Luo G., Long J., Zhang B., Liu C., Ji S., Xu J., Yu X., Ni Q.*: Quantum dots in cancer therapy. Expert Opin. Drug Deliv. 2012, 9, 47-58.
20. *Marsh M.* (ed.): Endocytosis. Oxford University Press 2001.
21. *Mi W., Tian W., Tian J., Jia J., Liu X., Dai J., Wang X.*: Synthesis of CdSe quantum dots in ethanol: A facile way to achieve photoluminescence with high brightness. Colloids and Surfaces A: Physicochem. Eng. Aspects, 417, 2013, 179-182.
22. *Naccache R., Rodríguez E. M., Bogdan N., Sanz-Rodriguez F., Cruz Mdel C., Fuente A. J., Vetrone F., Jaque D., Sole J. G., Capobianco J. A.*: High resolution fluorescence imaging of cancers using lanthanide ion-doped upconverting nanocrystals. Cancers (Basel). 2012, 4, doi: 10.3390/cancers4041067
23. *Nemade K. R., Waghuley S. A.*: UV–VIS spectroscopic study of one pot synthesized strontium oxide quantum dots. Results in Physics. 2013, 3, 52-54.
24. *Nwokolo C. U., Lewin J. F., Hudson M., Pounder R. E.*: Transmucosal penetration of bismuth particles in the human stomach. Gastroenterology 1992, 102, 163-167.
25. *Sharma R., Ghasparian A., Robinson J. A., McCullough K. C.*: Synthetic virus-like particles target dendritic cell lipid rafts for rapid endocytosis primarily but not exclusively by macropinocytosis. PLoS One. 2012, 7, doi: 10.1371/journal.pone.0043248
26. *Sonavane G., Tomoda K., Makino K.*: Biodistribution of colloidal gold nanoparticles after intravenous administration: effect of particle size. Colloids Surf Biointerfaces 2008, 66, 274-280.
27. *Sun L. D., Wang Y. F., Yan C. H.*: Paradigms and Challenges for Bioapplication of Rare Earth Upconversion Luminescent Nanoparticles: Small Size and Tunable Emission/Excitation Spectra. Acc. Chem. Res. 2014, [Epub ahead of print]
28. *Trefry J. C., Wooley D. P.*: Silver nanoparticles inhibit vaccinia virus infection by preventing viral entry through a macropinocytosis-dependent mechanism. J. Biomed. Nanotechnol. 2013, 9, 1624-1635.
29. *Volkheimer G. Z.*: The Phenonenon of persorption – history and facts. Arztl. Fortbild. Jena 1993, 87, 217-221.
30. *Wahab R., Tripathy S. K., Shin H.-S., Mohapatra M., Musarrat J., Al-Khedhairy A. A., Kaushik N. K.*: Photocatalytic oxidation of acetaldehyde with ZnO-quantum dots. Chem. Eng. J. 2013, 226, 154-160.
31. *Wang J., Yong W. H., Sun Y., Vernier P. T., Koeffler H. P., Gundersen M. A., Marcu L.*: Receptor-targeted quantum dots: fluorescent probes for brain tumor diagnosis. J. Biomed. Opt. 2007, 12, 044021.
32. *Wen Z., Zhao B., Song K., Hu X., Chen W., Kong D., Ge J., Bu Z.*: Recombinant lentogenic Newcastle disease virus expressing Ebola virus GP infects cells independently of exogenous trypsin and uses macropinocytosis as the major pathway for cell entry. Virol. J. 2013, 10, doi: 10.1186/1743-422X-10-331
33. *Yatsunenko S., Kaszewski J., Grzyb J., Pełech I., Godlewski M. M., Mijowska E., Narkiewicz U., Godlewski M.*: Impact of yttria stabilization on Tb^{3+} intra-shell luminescence efficiency in zirconium dioxide nanopowders. J. Phys. Condens Matter. 2013, 25, 194106, doi: 10.1088/0953-8984/25/19/194106
34. *Yuji M., Tsubata M., Chin K., Onishi S., Inamoto T., Qi W.-M., Warita K., Yokoyama T., Hoshi N., Kitagawa H.*: Persorption of luminal antigenic molecule and its specific antibody via apoptotic epithelial cells of intestinal villi and Peyer's patches into peripheral blood in rats. J. Vt. Med. Sci. 2006, 68, 1297--1305.

Corresponding author: dr Michał M. Godlewski, Nowoursynowska 159, 02-776 Warsaw, Poland; e-mail: mickgodl@hotmail.com